Impact of Late Quaternary climatic fluctuations on coastal systems: Evidence from high-resolution geophysical, sedimentological and geochronological data from the Java Island

Franto Novico, David Menier, Manoj Mathew, Mu Ramkumar, M. Santosh, Cipta Endyana, Kresna Tri Dewi, Indra Kurniawan, Clément Lambert, Evelyne Goubert

HAL Id: hal-03485730
https://hal.univ-brest.fr/hal-03485730

Submitted on 8 Jan 2024

1   **Impact of Late Quaternary climatic fluctuations on coastal systems:**

2   **Evidence from high-resolution geophysical, sedimentological and**

3   **geochronological data from the Java Island**

4   Franto Novico[1,2], David Menier[3,*], Manoj Mathew[4], Mu Ramkumar[5], M. Santosh[6,7], Cipta

5   Endyana[1], Kresna Tri Dewi[8], Indra Kurniawan[9], Clément Lambert[3], Evelyne Goubert[3],

6   Hendarmawan[1]

7   [1]Department of Engineering Geology, Padjadjaran University, 45363 Jatinangor, Indonesia

8   [2]Marine Geological Research and Development Center, Ministry of Energy and Mineral

9   Resources, 40174 Bandung, Indonesia

10   [3]Laboratoire Géoscience Océan, UMR CNRS 6538, Université Bretagne Sud, 56017 Vannes,

11   France

12   [4]Laboratoire Géoscience Océan, UMR CNRS/UBO/UBS 6538, IUEM, Université de Brest,

13   29280 Plouzané, France

14   [5]Department of Geology, Periyar University, 636011 Salem, India

15   [6]Department of Earth Sciences, University of Adelaide, Adelaide, SA 5005, Australia

16   [7]Beijing School of Earth Sciences and Resources, China University of Geosciences, 100083

17   Beijing, China

18   [8]Center of Geological Survey, Ministry of Energy and Mineral Resources, 40122 Bandung,

19   Indonesia

20   [9]Directorate of Water Resources, Ministry of Public Works and Housing, 12110 Jakarta,

21   Indonesia

22   *Corresponding author: david.menier@univ-ubs.fr (D. Menier).

Abstract

The major climatic oscillations during the Quaternary Period significantly influenced the evolution and distribution of ancient and modern coastal systems. Here we investigate the morphology and sedimentary infilling of submerged Late Quaternary incised valleys along the northern coast of Java Island (Indonesia) using high-resolution geophysical, sedimentological and geochronological data. Our results indicate that the spatial development and morphology of the incised valleys are predominantly controlled by Quaternary glacial–interglacial eustatic fluctuations, within a marked subsiding setting. The valleys were incised during prominent Quaternary lowstands and most of the valley fill was emplaced during the last postglacial sea level rise. The valley fill forms a transgressive succession, consisting mainly of fluvial deposits at the base (possibly amalgamated from older sequences) overlain by shallow marine sediments and capped by hemipelagic deposits. The valley-fill architecture is strongly dependent on the valley morphology (depth of incision, width of the valleys, and extent of the intertidal zone). The shallow marine deposits contained within the narrow and linear valleys are mostly aggrading muds. The vertical incision and valley formation was chiefly controlled by the extent of glacial sea-level fluctuations. The studied sections represent the continental-offshore extension of a paleodeltaic system. The implication of our work is that even in predominantly enclosed shallow marine systems that are located distal to the shelf break, the response of the sedimentary system and ensuing stratigraphic configuration can be effectively impacted by the rapid and abrupt Quaternary global climatic transition and eustatic sea-level fluctuations.

Keywords: Last Glacial Maximum; Java Sea; Incised Valleys; depositional controls; stratal morphology

1. Introduction

48 The Quaternary Period is characterized by rapid, large-scale and abrupt climatic oscillations

49 that strongly influenced the evolution and distribution of ancient coastal systems around the

50 world and continue to exert control until present-day (Adams et al., 1999; Elias, 2013;

51 Gornitz, 2021). The associated eustatic fluctuations predominantly generated arrays of incised

52 valleys during relative sea level lowstands which were inundated and filled during subsequent

53 relative sea level rise, inundated and infilled the incised valleys. Over the last 40 years, owing

54 to its scientific and economic significance, extensive research has been focused on the

55 stratigraphy and infilling of such incised valleys or paleochannels (Puchala et al., 2011; Wang

56 et al., 2020). Research conducted elsewhere has provided important geomorphologic as well

57 as stratigraphic information from regions such as the North and South American shelf (e.g.,

58 Dalrymple et al., 1994; Nordfjord et al., 2006; Moreira et al., 2019), northwest European shelf

59 (e.g., Allen and Posamentier, 1993 and 1994; Tesson et al., 2000; Chaumillon et al., 2010;

60 Menier et al., 2010; Martinez-Carreno and Garcia-Gil, 2017), northeastern Australian shelf

61 (e.g., Fielding et al., 2005), southwestern Huanghai shelf (e.g., Kong et al., 2011), South

62 African shelf (e.g., Green, 2009), eastern Indian coast (e.g., Dubey et al., 2019), Sunda shelf

63 in Southeast Asia (e.g., Hanebuth et al., 2009; Puchala et al., 2011; Horozal et al., 2021),

64 among others.

65 In Southeast Asia, the Sunda Shelf or Sundaland is an extension of the continental shelf and

66 includes the island of Java, the Malay peninsula, Sumatra, Borneo, Madura, Bali and their

67 surrounding smaller islands. It covers an area of approximately 1.85 million km². Its seas are

68 relatively shallow and was exposed several times during the Pleistocene (e.g., Emery et al.,

69 1972; Hanebuth et al., 2009) when Sumatra, Java, Borneo and the Malay peninsula were

70 connected and formed a single large landmass (Heaney et al., 1991; Voris, 2000; Bird et al.,

71 2005) (Fig. 1A). During the Last Glacial Maximum (LGM), ~26.5–19 ka BP, much of the

72 remaining Sundaland area was covered by savanna, grassland, lowland evergreen forests,

73   marshy grounds and crossed axially by the deeply incised 'rivers' feeding the late falling-

74   stage deltas that debouched close to the present-day shelf break of the Sundaland (Hanebuth

75   et al., 2009; Hanebuth et al., 2011; Puchala et al., 2011; Sathiamurthy and Rahman, 2017;

76   Irwanto, 2019). The Java Sea that today corresponds to a large and shallow sea of the Sunda

77   Shelf, which lies between the islands of Borneo to the north, Java to the south, Sumatra to the

78   west and Sulawesi to the east, was entirely exposed during the LGM (Clark et al., 2009). The

79   Java Sea was occupied by river valleys and channels that coursed to the shelf break located

80   toward the eastern part of Java. Currently, the northwestern region of the Java Sea hosts a

81   poorly-documented offshore sedimentary prism dominated by argillaceous deposits within a

82   rapidly subsiding geodynamic setting (Abidin et al., 2008, 2013 and 2015, Chaussard et al.,

83   2013; Husson et al., 2019). While it is recognized that this region has undergone various

84   phases of tectonic and eustatic fluctuations until recent-times (e.g., Zahirovic et al., 2016), a

85   detailed analysis of the sedimentary architecture and stratigraphic archive, which can

86   potentially encapsulate evidences of important environmental changes in response to

87   endogenic and exogenic forcing, remain less understood.

88   Here, we present a detailed description of the shallow sub-bottom stratigraphy of the offshore

89   section of northwest Java (Fig. 1B) using results obtained from shallow seismic surveys and

90   cores collected in 2015. These results, aided with radiocarbon ages provide insights into the

91   Pleistocene to Holocene transition events and the major climatic and eustatic controls on the

92   sedimentary organization within a subsiding shelf setting.

93   **2. Geological characteristics of Java and Java Sea**

94   **2.1. Structural setting**

95   Sundaland consists of a stable core of Paleozoic continental crust that was augmented in size

96   by tectonism and volcanism associated with subduction along the southern margin of the

97   continent, with episodes of uplift and subsidence affecting the entire Sunda Shelf (Bird et al.,

98   2005; Metcalfe, 2011). Java represents a volcanic arc built on the southernmost margin of the

99   continental Sunda Plate, due to the subduction of the oceanic Australia-Indian plate (Fig. 2A;

100   Hamilton, 1979). It is a structurally complex island attributable to a long history of accretion

101   of Gondwana-derived crustal blocks that led to a configuration of alternating highs and

102   transverse depressions (Haberland et al. 2014). The northern part of the Northwest Java Basin,

103   including the coastal area, is dominated by extensional faulting with minimal compressional

104   structures (Darman and Sidi, 2000; Sathiamurthy et al., 2006). It was formed by continuous

105   subsidence and southward tilting of the Sunda Plate since the Paleogene (Hamilton, 1979).

106   The subsidence is documented to have resulted in the development of the Pulau Seribu

107   carbonate platforms (Fig. 1B) and the NE-SW trending asymmetrical northwest Java basinal

108   area (Suyanto et al., 1977). Subsequent development of several sub-basins and basement

109   highs within the basin (Patmosukismo et al., 1974) was associated with N-S trending block

110   faulting (Adriansyah et al., 2002).

111   2.2. Geomorphology and seafloor sedimentary cover

112   Morphologically, the Java Sea is roughly rectangular in shape, located between Sumatra to the

113   west and Bali to the east. In the west, it is open to the Indian Ocean through the Sunda Strait

114   and the Karimata Strait, respectively. In the east, it has an open connection to the Flores Sea

115   and the Sulawesi Sea through the Makassar Strait (Durand & Petit, 1995; Genia et al., 2007).

116   The Java Sea including Jakarta Bay is a large (~310,000 km²), shallow sea (40–100 m water

117   depth) and the slope is toward the east at the edge of the Sunda Shelf. Seafloor surface

118   sediment of Indonesian waters including the Java Sea generally consists of cohesive fine-

119   grained sediments (Fig. 2).

120   Java presents an elongated morphology with a surface area of ~130,000 km^2 (~1000 km in

121   length and ~210 km wide). The coastline is structurally controlled and shows an irregular

122 morphology. Northern Java including the Jakarta Bay is in a transition area between the

123 volcanic arc and the extensional back-arc zone. This area is characterized by the flat alluvial

124 plain of the coastal zone. The southern parts of Java are occupied by volcanic mountains

125 where Mount Semeru is the highest (~36576 m). Java is drained by multiple rivers, with large

126 drainage basins in the north and small drainage basins in the south (Figure 3). The drainage

127 pattern is predominantly controlled by the volcanic arc and recent uplift (Marliyani, 2016).

128 **2.3. Sea level changes**

129 On a global scale, the development of Quaternary stratigraphy of continental shelves was

130 predominantly controlled by glacio-eustatic fluctuations (Suter et al., 2012). Hence, an

131 understanding of relative sea-level change may help to explain critical interactions in earth

132 environmental systems throughout the Quartenary (Shennan, 2018).

133 The Sundaland core is considered to be tectonically quiescent, as evidenced by the lack of

134 noticeable seismic activity of the fault systems. However, a recent biographical study on

135 organism divergence time (Husson et al., 2019) shows that Sundaland was subaerially

136 exposed before 400 ka and subsequently experienced subsidence at a rate of 0.2–0.3 mm yr^{-1}

137 (Sarr et al., 2019). The insights gained from Sarr et al. (2019), resulted in an updated

138 framework of sea level changes for Sundaland by combining variations of both glacio-eustatic

139 and subsiding activity.

140 During the LGM, when ice sheets were at their maximum, the glacio-eustatic depression of

141 the sea level by ~120 m had fully exposed the Sunda Shelf. Several previous studies (e.g.,

142 Bird et al., 2005; Sathiamurthy et al., 2006; Cannon et al., 2009; Sathiamurthy et al., 2017),

143 using sedimentological, geophysical and palynological data records from the LGM stage,

144 reconstructed the paleogeography of Sundaland along the areas from the South China Sea and

145 Malacca Strait to the Java Sea. The area was dominated by large fluvial drainage systems with

146   savanna and lowland evergreen vegetation in their catchment areas (Fig.1A). Sea level

147   changes seem to play a critical role in variability of the sedimentary successions in these areas

148   including the Jakarta Bay and the Java Sea.

149   The last marine flood that initiated ~19 ka BP had significant consequences on the

150   remobilization of sediments of the paleolandscapes associated with the vast coastal plain,

151   which occupied most of the present-day Java Sea. During this sea level rise, the new

152   hydrodynamic conditions led to a reorganization of the sedimentary architecture that initiated

153   with continental sedimentary regime to a mixed sedimentary system (i.e., both marine and

154   continental) and then culminated in an exclusively marine-dominated stratigraphic

155   architecture, to reach the current coastline of northern Java.

156

157   **3. Material and methods**

158   **3.1. Geophysical data acquisition and processing**

159   Two high-resolution reflection seismic (HRRS) single channel data records were used. The

160   first set of seismic profiles correspond to refined HRRS campaigns that were carried out in

161   June to July 2015, covering nearly the entire Jakarta Bay. The second set of seismic profiles

162   were obtained from the HRRS data acquisition campaign that was conducted in March 1990

163   (unpublished report by Kurnio et al., 1991) for the Java Sea (Fig. 1B). Both seismic records

164   were acquired by deploying a sparker system that could penetrate up to 250 ms TWTT.

165   Cheaspeake Sonarwiz 5 software was used for processing the single channel data by

166   completing the sea bottom track by noise attenuation, seismic signal gaining by Automatic

167   Gain Control and User Define Gain/Attenuation, bandpass filtering through frequency

168   selection to have a better resolution of seismic reflectors at upper layers of sub-sea bottom and

169   seismic trace stacking by increasing the ratio of signal/noise to obtain a better quality of the

170   reflectors. The time-depth conversion for sediment unit boundaries was assumed using an

171   internal velocity of 1600 m/s beneath the seafloor (Puchala et al., 2011; Martínez-Carreño and

172   García-Gil, 2017). Thus, 200 m depth was reached with some approximately visible

173   reflectors. Survey positioning was achieved with a differential global positioning system

174   (DGPS) using CNAV 3050. The seismic reflectors were analyzed following the procedures

175   enlisted by Mitchum and Vail (1977), Brown and Fisher (1980), Posamentier et al. (1988),

176   Posamentier and Vail (1988), and Catuneanu (2019).

177   **3.2. Sediment cores**

178   Ten boreholes (BH-01–BH-10) were drilled (Figs. 1C and 2B) around the Jakarta Bay. The

179   borehole, BH-10, has the deepest water depth (22 m below Lowest Astronomical Tide -LAT),

180   while the others varied from 14 to 19 m water depth below LAT. Among the 10 boreholes, the

181   drilling depth of BH-02 and BH-07 reached 150 m below the sea bed and both boreholes were

182   located in the middle of the bay (Fig. 1C and Table 1). The other boreholes were drilled to a

183   depth of 60 m below the seafloor. The retrieved sediment cores were used to describe the

184   lithology, microfauna and organic matter (e.g., fragments of fossilized wood, rootlets,

185   charcoal, etc.) to decipher the depositional environments, which were interpreted based on

186   granulometric analyses (30 g dry samples were sieved for grain sizes 2 mm, 500 μm, 250 μm

187   and 63 μm) and microfossil analysis (using stereo zoom Zeiss Stemi SV 11) following

188   standard procedures.

189   **3.3. AMS ^{14}C dating**

190   The selected samples for radiocarbon dating were analyzed with Accelerator Mass

191   Spectrometry at the Radiocarbon Laboratory, University of Arizona, USA. Each age

192   measurement was conducted on shell fragments and organic matter extracted from the cores.

193   All radiocarbon dates are given in years before present/1950 (BP) (Smith et al., 2011; Reimer

194 et al., 2013). Radiocarbon dates with a "measured radiocarbon age" older than 46,400 yrs BP

195 are outside the detection limits and are not calibrated; thus, these ages are shown as > 46,400

196 yrs BP (Table. 2).

197 **4. Results**

198 **4.1. Interpretation of seismic reflection configuration patterns and seismic stratigraphy**

199 The seismic profiles were analyzed in terms of continuity, amplitude, configuration and

200 termination of reflectors following Mitchum et al. (1977) and Catuneanu (2019). This was

201 followed by the recognition of seismic units and description of the recognized units along

202 with their boundaries (unit boundary - UB). The characteristics of the acoustic facies are

203 summarized in Table 3 for the seismic units observed in the offshore zone and identified in

204 boreholes BH-02 and BH-07.

205 To illustrate the Holocene infilling of the incised valleys from the Jakarta Bay to the Java Sea,

206 we selected five seismic profiles that are located in the central part of the study zone.

207 In the five profiles (sparker profiles: L-42, CL-06B, L-C7, L-C8 and L-X), located at water

208 depths ranging from 5 to 50 m, seven seismic units, i.e., U1–U7, from the base towards the

209 top, were identified in the sedimentary infilling of the incised valleys (Fig. 4 and Table 3).

210 These units are illustrated on the selected profiles, except for Units 1, 2 and 3, which are only

211 adequately visible on L-42. Units 1 and 2 are characterized by discontinuous reflectors with

212 an acoustically opaque configuration.

213 Unit 1 (U1) is located in the basal part (Fig. 4A) and displays a thickness of >25 ms TWTT

214 (>20 m). The reflectors of U1 demonstrates very poor continuity, low frequency and low

215 amplitude (Table 3). The reflection configuration is aggrading sub-parallel with attenuated

216 zones (acoustically opaque) as a result of subsurface gas. It should be noted that this area has

217   been shown to contain acoustically turbid zones, which are related to the presence of gas in

218   organic-rich sediments (e.g., Schubel, 1974; Baltzer et al., 2005).

219   Unit 2 (U2) presents an acoustic thickness varying from 20 to 35 ms TWTT (~16 m to 28 m).

220   Continuity, amplitude and frequency in seismic facies range from low to medium and very

221   poor at some parts with acoustic turbidity (Table 3). Reflector configuration displays

222   aggrading sub-parallel to parallel patterns associated with a shallow marine environment, such

223   as a deltaic depositional system.

224   Unit 3 (U3) exhibits an acoustic thickness varying between 35 ms to 60 ms TWTT (~28 m to

225   48 m). U3 is characterized by aggrading reflectors in the sedimentary prism wedging

226   morphology systems towards the south and the north, particularly in the lower section of the

227   seismic line L42. This seismic facies is interpreted as a deltaic depositional system.

228   Unit 4 (U4) overlies U3 (Figs. 4 and 5) and has an acoustic thickness varying between 50 ms

229   and 70 ms TWTT (~40 m to 64 m). The reflectors show very poor to moderate continuity and

230   the amplitude and frequency are medium (Table 3). The top of the unit is bounded by an

231   erosional surface. The internal reflectors show corrugated reflector stacking pattern, probably

232   due to the prevalence of superimposed subaqueous lobes within a deltaic system, and some

233   erosional surfaces, which in turn are located at the southern and northern parts. The seismic

234   facies could suggest that U4 comprises an alluvial plain depositional environment (Reineck

235   and Singh, 1980; Catuneanu et al., 2009; Catuneanu, 2019).

236   Unit 5 (U5) overlies U4 with an acoustic thickness varying between 5 ms to 50 ms (~4 m to

237   40 m) and is bounded by erosional surfaces on the top and bottom (Figs. 4 and 5). The unit

238   extends laterally to a planar geometry. The continuity of seismic facies is very poor to poor

239   corresponding to acoustic attenuation and demonstrates an oblique-aggrading subparallel

240   geometry, while amplitude and frequency are low to high (Table 3). Aggrading subparallel

241 seismic reflector geometry is commonly found beside discontinuous reflectors that could

242 indicate existing gas pockets. This unit presents a general organization of horizontal reflectors

243 with some downlap and onlap in a few places. Using indications from the seismic facies, the

244 depositional environment of U5 is interpreted as a delta plain with some parts containing

245 alluvial channels and tidal flat sediments (Brown and Fisher, 1980; Reineck and Singh, 1980;

246 Catuneanu et al., 2009; Catuneanu, 2019).

247 The next unit, U6, presents an acoustic thickness of 5 ms to 40 ms TWTT (~4 m to 32 m)

248 (Figs. 4 and 5). This unit reveals acoustic facies that are characterized by aggrading parallel

249 and progradation pattern of poor continuity, and low to high frequency with very low to high

250 amplitude (Table 3). The base of U6 corresponds to a subaerial unconformity and

251 demonstrates flat upper layers that overlie clinoform deposits in some parts (Figs. 4 and 5),

252 which intersects U5 with a divergent filling pattern. The variation in thickness of this unit is

253 associated with incised channels and U6 is interpreted as delta front deposits within a shallow

254 marine setting (Reineck and Singh, 1980; Dalrymple et al., 2003; Catuneanu et al., 2009;

255 Catuneanu, 2019).

256 Unit 7 (U7) is the most recent seismic unit which overlies U6 (Figs. 4 and 5). The seismic

257 facies show medium to good continuity with good amplitude and medium frequency. Seismic

258 reflector configuration is predominantly aggrading parallel (Table 3). The acoustic thickness

259 ranges between 5 ms to 30 ms TWTT (~4 m to 24 m). The depositional environment of U7 is

260 interpreted as a subaqueous fan delta in the south-central and eastern parts that can be

261 associated with existing river mouths and a shoreface setting toward the north as seen in the

262 modern bathymetric map of the study area.

263 **4.2. Lithofacies description and correlation from sediment cores**

264   Lithofacies description of the recognized seismic units was conducted on selected cores, i.e.,

265   BH-02, BH-04, BH-05, BH-06, BH-07 and BH-09 (Figs. 2B and 6). It is evident from the

266   sparker profile L-42 (Fig. 4A) that these cores represent a complete and continuous record of

267   stratigraphic successions in units U2 to U7, and thus provide the optimal opportunity to

268   investigate the sedimentary infilling history of the study area. U2 was recognized at a depth of

269   130–150 m and consists of dark grey to olive grey silt and clay, and medium to dark grey

270   very-fine to fine-grained sand and the depositional environment indicated an inner shelf

271   setting. U3 comprises of sediments that correspond to grey clay and dark grey medium-

272   grained sand as seen in BH-02 and BH-07 and gathering information from the seismic facies,

273   this unit is interpreted as being deposited in a deltaic setting. The lithology of U4, as seen in

274   cores BH-04 to BH-09, and identified at a depth of 46–100 m below the seabed, is

275   characterized by dark grey to olive grey silt with traces of clay, medium to coarse grain

276   greyish brown sand and silt with traces of clay that indicate a shallow marine to alluvial plain

277   depositional environment. Core description of boreholes BH-04 and BH-09 (Fig. 6) reveal

278   that U5 consists predominantly of greyish brown to brown sand and brownish grey silt and

279   clay. Informed by the seismic facies and lithofacies, we interpret the depositional environment

280   of U5 as a delta plain with some parts containing alluvial channels and tidal flat sediments.

281   The sediments of U6, witnessed in the boreholes BH-05 and BH-07, reveal dark grey to black

282   sand, medium to coarse grained sand and dark grey mud with some medium grain sand. The

283   basal sequence boundary is overlain by yellowish-brown medium grain sand, reversed graded

284   bedding, containing shell fragments, which denote a shallow marine to deltaic depositional

285   environment. U7 occupies the stratigraphic succession between 0 to 12 m and consists of

286   yellowish-grey clay with medium grained sand containing visually ±10% of shell fragments

287   and depositional environment is interpreted as a shallow offshore environment

288   **4.3. Micropaleontological indices**

289   Microfossils were identified and described from cores BH-02, and BH-07 (Table 4).

290   The dominant benthic foraminifera taxa (i.e., *Ammonia* spp .; *Asterorotalia* spp.) (Fig. 7 and

291   Table 4) in U2 seem to indicate a coastal waters environment. *Ammonia tepida* is indeed

292   known to be tolerant to continental organic matter and freshwater inputs in the southwestern

293   Pacific region (Debenay, 2012). *Asterorotalia* spp. is a typical warm water epifaunal benthic

294   foraminifera well represented in riverine influx dominated coastal domain (Panchang and

295   Nigam, 2012; Saraswat et al., 2017). Microfossil barren zones are observed in U4 in both BH-

296   02 and BH-07. A gradual increase in benthic foraminifera, especially *Elphidium* spp.,

297   *Operculina* spp. and *Quinqueloculina* spp. is seen in the upper parts of U4 and in U5 within

298   BH-07, while ostracods are very rare in these two units (Table 4). Similarly, in BH-02, the

299   lack of ostracods is evident in U4 and U5, while rare occurrences of *Elphidium* spp.,

300   *Pseudorotalia* spp. and *Quinqueloculina* spp. is noticed in upper parts of U4. U6, similar to

301   U3, entails an abundance of various species of ostracods and benthic foraminifera and this

302   could be indicative of a shallow marine setting (Table 4). U7 reveals the presence of some

303   marine benthic foraminifera taxa found in modern warm marine waters of southwestern

304   Pacific Ocean (e.g. *Dendritina* spp., *Spiroloculina* spp., Hohenegger et al., 1999; Debenay,

305   2012). *Dendritina* spp. is indeed a full marine species frequently found abundant in regions

306   protected from extreme hydrodynamic forcing.

307

308   **4.4. Radiocarbon ages**

309   A total of 3 cores (i.e., BH-05, BH-06 and BH-07) were sampled for radiocarbon dating. The

310   dating analysis from a sample recovered at 134.5 m depth of BH-07 and pertaining to U2

311   revealed an age of > 49,900 ka BP.

312   In the same core, ^{14}C dating results (Table 2) of samples at 77 m depth and 56.2 m depth, and

313   within U4, presented ages of > 46.4 ka BP and 41.8 ± 1.5 cal ka BP, respectively.

314   The result of radiocarbon dating applied on shell materials of the sub-sample from 14.3 m

315   below the seabed from BH-06 revealed an age of 8461 ± 29 cal yrs BP (Table 2).

316   The dating applied on molluscan shell collected at 7 m depth below seafloor from BH-05

317   returned an age of 3,308 ± 24 cal yrs BP (Table 2).

318   **5. Discussion**

319   **5.1. Sequence stratigraphic framework**

320   While all the depositional units are not equally preserved in all the studied valleys, a general

321   stratigraphic scheme can be drawn that applies over the entire zone or system.

322   The chronology of the complete succession remains speculative for Units 1, 2 and 3 except

323   for the upper units (U4–7), wherein, the formations indicate ages ranging from the Pleistocene

324   to Holocene. U4 that signifies the falling stage systems tract shows a first stage of incision

325   and is characterized by alluvial deposits (Figs. 4 and 6), which indicate ages of > 46.4 ka BP

326   and 41.8 ± 1.5 cal ka BP (MIS 3) (Table 2) and we interpret this sequence to be associated

327   with the accumulation of regressional deposits following the persistent drop of relative sea

328   level since MIS 5e. The microfossil assemblages (benthic foraminifera and ostracods) within

329   U4 show a dramatic decline in BH-02 and BH-07 (Table 4) that further supports the

330   interpretation of relative sea level drop and subaerial exposure of the shelf. U5 incorporates

331   mixed fluvio-estuarine deposits that could have been emplaced initially under lowered relative

332   sea levels, during which, regressional alluvial channel deposits continued to accumulate and

333   sealed the first incisional features. Incision synchronously propagated across these deposits,

334   and later as relative sea level began to gradually increase there could have been reduced

335   incisional capacity with aggradation of sediments due to a rise in base level and some filling

336 of the incised system, and owing to these evidences, we deduce U5 to represent the lowstand

337 systems tract. The gradual rise in sea level and estuarine sedimentation is corroborated by the

338 increase in population of brackish and saline water favoring benthic foraminifera species such

339 as *Elphidium* spp., *Operculina* spp. and *Quinqueloculina* spp. in BH-07. U6, demonstrating an

340 age of 8461 ± 29 cal yrs BP (Table 2) in the intermediate part of the sequence and which lies

341 above the transgressive surface, consists of shallow marine sediments that may have been

342 deposited during rapid transgression after ~15 ka BP, which could efficiently preserve the

343 preceding fluvial deposits, and we posit that this unit elucidates the transgressive systems

344 tract. Lastly, the Holocene sediments forming the hemipelagic drape of U7 that overlie the

345 maximum flooding surface represent the highstand systems tract.

346 **5.2. Valley morphology**

347 As defined by the seismic data shown in figure 5 (Fig. 1B for location), the valleys run

348 parallel to the coast and are between 1 and 10 km long. They follow a regional slope towards

349 the shelf break and reach maximum depths of ~30 to 40 m. These valleys are increasingly

350 wide towards the east, particularly where several valleys converge, and are linked to the

351 confluence of fluvial channels. Indeed, there could have been high rates of sedimentation,

352 channel flow and drainage discharge which could possibly explain the processes of alluviation

353 and incisional dynamics that promoted the notable widening of the emerging valleys in the

354 Java Sea (Fig. 8), that are mainly controlled by global sea level changes during the LGM

355 (Voris et al, 2000; Hanebuth et al., 2004; Clark et al, 2009; Sar et al, 2019).

356 These valleys, filled by marine transgressive deposits (U6–shallow marine), are underlain by

357 mixed fluvio-estuarine formations of weakly consolidated origin (U5–lowstand channel fill),

358 the facies of which are mainly fine to medium grained.

359 The morphology of the valleys demonstrates generally a flat bottom and markedly steep edges

360 (Fig. 5).

361   The morphology with a flat bottom and marked edge can be explained by the lithological

362   nature of the incised unit (U5), consisting of weakly consolidated and easily remobilized

363   alluvial plain deposits, and conversely as a zone where the potential for incision is very low

364   given the low to medium slopes in a region very far from the continental slope (Fig. 8A).

365   The incision depths of ~8 m to 32 m, (Fig. 5) are of the same order as those documented from

366   other parts of the world, for example, on the platforms of the American east coast (Thomas

367   and Anderson, 1994; Foyle and Oertel, 1997), the Bay of Biscay (Lericolais et al., 2001;

368   Chaumillon et al., 2008; Chaumillon et al. 2010; Menier et al., 2010; Estournès et al., 2012;

369   Menier et al., 2014; Martínez-Carreño and García-Gil, 2017), the Mediterranean (Tesson et

370   al., 2010; Tesson et al., 2015), India (Dubey et al., 2019) and also in Southeast Asia

371   (Hanebuth, et al., 2009; Puchala et al., 2011; Alqahtani, et al., 2015; Wang et al., 2020;

372   Horozal et al., 2021).

373   **5.3. Depositional evolution**

374   The main stratigraphic units recognized across the study area are composed of continental

375   formations (U4 and U5) that transitions upward to shallow marine deposits (U6 and U7). This

376   interpretation is also confirmed by the succession of fossil foraminifera faunas, from taxa that

377   are indicative of environments under continental influence (*e.g. Asterorotalia* spp.) to those

378   that are indicators of shallow coastal waters (*e.g. Dendritina* spp., *Spiroloculina* spp.,

379   *Operculina* spp.) (Fig. 7 and Table 4). The core and the major parts of the valley fills are

380   composed of alluvial deposits (U5) and shallow marine deposits (U6 and U7), and the vertical

381   facies succession is predominantly deposited within a transgressive setting.

382   In our proposed model of valley morphogenesis, the supposed thalweg, which overlays the

383   erosional surface UB-4, is dated at 41800 +/- 1500 cal. age BP, which corresponds to the last

384   and deepest incision (pre-LGM incision), and therefore, the overlaying fluvial deposits (U5)

385   could be younger than 25 ka. Based on deductions implied in previous studies (e.g.,

386   Posamentier and Allen, 1999; Posamentier, 2001), the alluvial channels more than likely

387   formed when the shelf was not fully subaerially exposed and the lowstand fluvial system was

388   incapable of substantially efficient downcutting, both laterally and vertically.

389   On the seismic records (Fig. 3B and Table 3) U4 seem to illustrate an irregular and oblique

390   aggrading subparallel or wavy reflector geometry and we interpret it as interfluves or bars,

391   dominated by sandy to silt-argillaceous facies established during the marine isotopic stage 3

392   (Fig. 9).

393   Unit 5 is interpreted to consist of lowstand channel fill deposits that accumulated during

394   periods of significant drops in sea level but the majority during the post lowstand system tract

395   (LST), which was lower than present-day in this zone (Fig. 9). Our results clearly highlight

396   the occurrence of alluvial channel deposits and nearshore tidal flat sediments that are

397   explicitly indicative of a shift from a relatively sand-rich lowstand system to a clay-rich

398   nearshore sediment as mention in Table 4. Gathering consensus from the global and Sunda

399   shelf sea level curves (Fig. 9), the transition from a fluvial to a shallow marine setting in our

400   data could correspond to the post-LGM abrupt and rapid sea level rise induced by

401   deglaciation. Furthermore, our inference of an abrupt and rapid rise in sea level is congruent

402   with previous findings (Hanebuth et al., 2000) of an accelerated increase in eustatic levels in

403   the northern Sunda Shelf during the MWP 1A (meltwater pulse) event that commenced at

404   ~14.7 ka and terminated before ~13.8 ka, including an abrupt rise of up to ~16 m within a

405   span of 300 years that occurred between 14.6–14.3 ka cal BP (Hanebuth et al., 2000).

406   Unit 6, dated at ~8461 +/- 29 cal. age BP, which mainly rests above Unit 5, is interpreted as

407   deposited in the course of the last sea level rise over the area (Fig. 8). As the fluvial valleys

408   were flooded by the rising sea levels, sediment supply could not keep pace with the increase

409   of accommodation space, and this would explain the aggrading nature of Unit 6. The very

410   homogeneous structure of Unit 6 and the inferred fine-grained sedimentation would point to a

411 wave-dominated bay (Dalrymple et al., 1994). While there is an inexistence of sandy barriers

412 in the seismic record, the Java Sea seems to be a sector that was very calm, favoring low-

413 energy sedimentation comparable to that in estuarine central basins (lagoonal basins). Further

414 expanding on our sedimentological and seismic data, we favor the interpretation of very calm

415 and low-energy conditions in the Java Sea during the deposition of Unit 6. We base this on an

416 additional line of evidence, viz. the preservation of Unit 5 could be plausible only under rapid

417 transgression and placid hydrodynamic environments. This can effectively weaken potential

418 erosional processes, given that ubiquitously, the efficient preservation of lowstand fluvial

419 deposits, subsequent to erosion during transgression and reworking by inclement

420 hydrodynamic conditions, would be, at best, in patches (Allen, 1991; Allen and Posamentier,

421 1993; Posamentier, 2001).

422 Unit 7 is interpreted as offshore muds aggrading above the estuarine valley fills as the first

423 succession overlaying UB-6. It rests above the maximum flooding surface that truncates all

424 the units below (Figs. 4 and 10). The unit is dated at ~3308 +/- 24 yr BP, and is composed of

425 Holocene-age hemipelagic drape. U7 was emplaced during a full transgression over the area,

426 inasmuch as it overlaps most of the valley interfluves.

427 **6. Conclusions**

428 Two remarkable incisions are identified in the Java Sea shelf. The first incision occurred

429 during the sea level drop of the marine isotopic stage 3, which was later sealed by

430 lowstand alluvial channel deposits. These deposits were re-incised during the LGM,

431 creating the second incisional surface. This discontinuity does not intersect the Upper

432 Pleistocene incision, indicating a relatively low incision potential, in a context of rapid sea

433 level rise within very sheltered hydrodynamic conditions.

434 The incised valleys demonstrate a wide and flat bottom morphology along with very steep

435 edges owing to low velocity channel flow and shallow paleo-topographic gradients. The

436   sedimentary infill of the incised valleys indicates the continent-offshore extension of the

437   paleodeltaic system, complete with variable facies characteristics and variable rates of

438   deposition. Influences of regional slope and hydrodynamics are recognized to have

439   exercised control over the spatial distribution of facies types as well as grain sizes of the

440   facies types.

441   Prevalence of major river systems that drained the Sundaland Craton that advanced over

442   former offshore regions during LGM created an extensive incised valley and associated

443   geomorphic-sedimentary infill.

Author Contributions

445   Author Contributions: Conceptualisation: F.N., D.M., M.M., H. and C.E.; methodology: F.N.,

446   D.M., R.K. and M.S.; field investigation: F.N. and I.K.; manuscript preparation: F.N., D.M.,

447   M.M., M.R. and H.; review and editing: F.N., D.M., M.M., M.R., M.S. and C.E.; figures:

448   D.M., M.M., F.N.,. and C.E.; microfossil analysis: F.N. and K.T.D.

References

Abidin, H.Z., Andreas, H., Djaja, R., Darmawan, D., Gamal, M., 2008. Land subsidence

    characteristics of Jakarta between 1997 and 2005, as estimated using GPS surveys.

    GPS Solutions 12, 23-32.

Abidin, H.Z., Andreas, H., Gumilar, I., Sidiq, T.P., Fukuda, Y., 2013. On the roles of

    geospatial information for risk assessment of land subsidence in urban areas of

    Indonesia. In: Zlatanova, S., Peters, R., Dilo, A., Scholten, H. (eds.), Intelligent

    Systems for Crisis Management. Lecture Notes in Geoinformation and Cartography.

    Springer, Berlin, Heidelberg, 277-288.

Abidin, H.Z., Andreas, H., Gumilar, I., Brinkman, J.J., 2015. Study on the risk and impacts of

    land subsidence in Jakarta. Proceedings of the International Association of

    Hydrological Sciences 372, 115–120.

Adams, J., Maslin, M., Thomas, E., 1999. Sudden climate transitions during the Quaternary.

    Progress in Physical Geography 23(1), 1-36.

Adriansyah, A., McMechan, G.A., 2002. Case History, Analysis and Interpretation of seismic

    data from thin reservoirs: Northwest Java Basin, Indonesia. Journal of Geophysics 67

    (1), 14-26.

Allen, G.P., 1991. Sedimentary processes and facies in the Gironde estuary: A Recent model

    for macrotidal estuarine systems. In: Smith, D.G., Reinson, G.E., Zaitlin, B.A. and

    Rahmani, R.A. (eds.), Clastic tidal sedimentology. Canadian Society of Petroleum

    Geologists Memoir 16, 29–40.

482   Allen, G.P., and Posamentier, H.W., 1993, Sequence stratigraphy and facies model of an

483   incised valley fill: the Gironde Estuary, France. Journal of Sedimentary Petrology 63,

484   378–391.

485   Allen, G.P. and Posamentier, H.W. 1994. Transgressive facies and sequence architecture in

486   mixed tide- and wave-dominated incised valleys: example from the Gironde estuary.

487   France. In: Dalrymple, R.W., Zaitlin, B.A. and Boyd, R. (eds.), Incised valley

488   systems: origin and sedimentary sequences. Society of Economic Paleontologists and

489   Mineralogists, Special Publications 51, 225-240.

490   Alqahtani, F.A., Johnson, H.D., Jackson, C.A.-L, Som, M.R.B., 2015. Nature, origin and

491   evolution of a Late Pleistocene incised valley-fill, Sunda Shelf, Southeast Asia.

492   Sedimentology 62, 1198–1232.

493   Baltzer, A., Tessier, B., Nouze, H., Bates, R., Moore, C., Menier, D., 2005. Seistec seismic

494   profiles: A tool to differentiate gas signatures. Marine Geophysical Researches 26,

495   235-245.

496   Bird, M.I., Taylor, D., Hunt, C., 2005. Palaeoenvironments of insular Southeast Asia during

497   the Last Glacial Period: a savana corridor in Sundaland? Quaternary Science Reviews

498   24, 2228-2242.

499   Brown, L.F. and Fisher, W.L., 1980. Seismic-stratigraphic interpretation of depositional

500   systems and its role in petroleum exploration. AAPG Continuing Education Course

501   Notes Series 16, 1-181.

502   Catuneanu, O., Abreu, V., Bhattacharya, J.P., Blum, M.D., Dalrymple, R.W., Eriksson, P.G.,

503   Fielding, C.R., Fisher, W.L., Galloway, W.E., Gibling, M.R., Giles, K.A., Holbrook,

504   J.M., Jordan, R., Kendall, C.G.St.C., Macurda, B., Martinsen, O.J., Miall, A.D., Neal,

505   J.E., Nummedal, D., Pomar, L., Posamentier, H.W., Pratt, B.R., Sarg, J.F., Shanley,

506   K.W., Steel, R.J., Strasser, A., Tucker, M.E., Winker, C., 2009. Towards the

507   standardization of sequence stratigraphy. Earth-Science Reviews 92, 1-33.

508   Catuneanu, O., 2019. Scale in sequence stratigraphy. Marine and Petroleum Geology 106,

509   128–159.

510   Chaumillon, E., Proust, J.N., Menier, D., Weber, N., 2008. Incised-valleys morphologies and

511   sedimentary-fills within the inner shelf of the Bay of Biscay (France): A synthesis.

512   Journal of Marine Systems 72, 383-396.

513   Chaumillon, E., Tessier, B., Reynaud, J.Y., 2010. Stratigraphic records and variability of

514   incised valleys and estuaries along French coasts. Bulletin de la Société Géologique de

515   France 181, 75-85.

516   Chaussard, E., Amelung, F., Abidin, H., Hong, S-H., 2013.Sinking cities in Indonesia: ALOS

517   PALSAR detects rapid subsidence due to ground water and gas extraction. Remote

518   Sensing of Environment 128, 150-161.

519   Clark, P.U., Dyke, A.S., Shakun, J.D., Carlson, A.E., Clark, J., Wohlfarth, B., Mitrovica, J.X.,

520   Hostetler, S.W., McCabe, A.M., 2009. The Last Glacial Maximum. Science 325, 710-

521   714.

522   Dalrymple R.W., Boyd, R., Zaitlin, B.A., 1994. History of research, types and internal

523   organization of incised-valley systems: introduction to the volume. In: Dalrymple,

524   R.W., Boyd, R.J., Zaitlin, B.A. (eds.), Incised-valley systems: origin and sedimentary

525   sequences. Society for Sedimentary Geology special publication 51, 5–12.

526   Dalrymple, R.W., Baker, E.K., Harris, P.T., Hughes, M.G., 2003. Sedimentology and

527   stratigraphy of a tide-dominated foreland-basin delta (Fly River, Papua New Guinea).

528   In: Sidi, F.H., Nummedal, D., Imbert, P., Darman, H., Posamentier, H.W. (eds.),

529   Tropical Deltas of Southeast Asia-sedimentology, Stratigraphy, and Petroleum

530   Geology. SEPM 76, 147-173.

531   Darman, H. and Sidi, F.H., 2000; An outline of the geology of Indonesia. Indonesian

532   Association of Geologists, IAGI, Jakarta, 192 pp.

533   Dubey, K.M., Chaubey, A.K., Mahale, V.P., Karisiddaiah, S.M., 2019. Buried channels

534   provide keys to infer Quaternary stratigraphic and paleo-environmental changes: A

535   case study from the west coast of India. Geoscience Frontiers 10, 1577-1595.

536   Durand, J.R. and Petit, D., 1995. The Java Sea environment. in: BIODYNEX: Biology,

537   Dynamics, Exploitation of the small pelagic fishes in the Java Sea. Potier, M. and

538   Nurhakim, S. (eds.), Java Sea Pelagic Fishery Assessment Project. AARD/ORSTOM,

539   14-38.

540   Elias, S.A., 2013. The Quaternary. Reference Module in Earth Systems and Environmental

541   Science, Elsevier. DOI: https://doi.org/10.1016/B978-0-12-409548-9.05350-1.

542   Emery, K.O., Uchupi, E., Sunderland, J., Uktolseja, H.L, Young, E.M., 1972. Geological

543   structure and some water characteristics of the Java Sea and adjacent continental shelf.

544   CCOP Technical Bulletin 6, 197-221.

545   Estournès, G., Menier, D., Guillocheau, F., Le Roy, P., Paquet, F. and Goubert, E., 2012. The

546   paleo-Etel River incised valley on the Southern Brittany inner shelf (Atlantic coast,

547   France): Preservation of Holocene transgression within the remnant of a middle

548   Pleistocene incision? Marine Geology 329-331, 75–92.

549   Fielding, C.R., Trueman, J.D., Alexander, J., 2005. Sharp-based, flood dominated mouth bar

550   sands from the Burdekin River Delta of northeastern Australia: extending the spectrum

551   of mouth-bar facies, geometry, and stacking patterns. Journal of Sedimentary Research

552   75, 55–66.

553 Foyle, A.M. and Oertel, G.F., 1997. Transgressive systems tract development and incised-

554   valley fills within a Quaternary estuary shelf system: Virginia inner shelf, USA.

555   Marine Geology 137, 227–249.

556 Genia, A.N., Nugroho, A.S., Olugbenda, J.O., 2007. Introduction to Java Sea. Oceanography.

557   Stavanger, University of Stavanger.

558 Gornitz, V., 2021. Timescales of climate change. In: Alderton, D., Elias, S.A. (Eds.),

559   Encyclopedia of Geology (second edition). Academic Press, pp. 318-327.

560 Green, A.N., 2009. Palaeo-drainage, incised valley fills and transgressive systems tract

561   sedimentation of the northern KwaZulu-Natal continental shelf, South Africa, SW

562   Indian Ocean. Marine Geology 263, 46-63.

563 Haberland, C., Bohm, M., Asch, G., 2014. Accretionary nature of the crust of Central and

564   East Java (Indonesia) revealed by local earthquake travel-time tomography. Journal of

565   Asian Earth Sciences 96, 287–295.

566 Hamilton, W., 1979. Tectonics of the Indonesian region. United State of Geological Survey,

567   Washington, 1078 pp.

568 Hanebuth, T., Stattegger, K., Grootes, P.M., 2000. Rapid flooding of the Sunda Shelf: A Late-

569   Glacial sea-level record. Science 288, 1033-1035.

570 Hanebuth, T.J.J., Stattegger, K., Bojanowski, A., 2009. Termination of the last glacial

571   maximum sea-level lowstand: the Sunda-Shelf data revisited. Global and Planetary

572   Change 66, 76-84.

573   Hanebuth, T.J.J, Voris, H.K, Yokoyama, Y., Saito, Y., Okuno, J., 2011. Formation and fate of

574   sedimentary depocentres on Southeast Asia's Sunda Shelf over the past sea-level cycle

575   and biogeographic implications. Earth-Science Reviews 104, 92-110

576   Heaney, L.R., 1991. A Synopsis of Climatic and Vegetational Change in Southeast Asia.

577   Climatic Change 19, 53–61.

578   Horozal, S., Chae, S., Seo, J.M., Lee, S.M., Han, H.S., Cukur, D., Kim, D.G., Son, J.H., 2021.

579   Quaternary evolution of the southeastern Korean continental shelf, East Sea: Paleo-

580   incised valley and channel systems. Marine and Petroleum Geology 128, 105011.

581   Husson, L., Boucher, F.C., Sarr, A.-C., Sepulchre, P., Cahyarini, S.Y., 2019. Evidence of

582   Sundaland's subsidence requires revisiting its biography. Journal of Biogeography 47,

583   843-853.

584   Irwanto, D., 2019. Sundaland: Tracing the cradle of civilizations. Indonesia Hydro Media,

585   386 pp.

586   Kong, X.H., Liu, J., Du, Y.S., Wen, C., Xu, G., 2011. Seismic geomorphology of buried

587   channel systems in the western South Huanghai Sea: retrodiction for

588   paleoenvironments. Acta Oceanologica Sinica 30, 47-58.

589   Kurnio, H., Ilahude, D., Prawirasastra, R., Suprijadi, Kuntoro and Arifin, L., 1991. A report of

590   marine geological and geophysical investigation of the Java Sea (Map sheet 1210).

591   Unpublished report.

592   Lericolais, G., Berne, S., Fenies, H., 2001. Seaward pinching out and internal stratigraphy of

593   the Gironde incised valley on the shelf (Bay of Biscay). Marine Geology 175, 183-

594   197.

595   Marliyani, G.I., 2016. Neotectonics of Java, Indonesia: Crustal Deformation in the Overriding

596   Plate of an Orthogonal Subduction System. PhD Thesis, Arizona University, 371pp.

597   Martínez-Carreño, N. and García-Gil, S., 2017. Reinterpretation of the Quaternary

598   sedimentary infill of the Ría de Vigo, NW Iberian Peninsula, as a compound incised

599   valley. Journal of Quaternary Science Reviews 173, 124-144.

600   Menier, D., Reynaud, J.Y., Proust, J-N., Guillocheau, F., Guennoc, P., Tessier, B., Bonnet, S.,

601   Goubert, E., 2006. Basement control on shaping and infilling of valleys incised at the

602   southern coast of Brittany, France. S.E.P.M. Society for Sedimentary Geology, Special

603   Publication 85, 37-55.

604   Menier, D., Tessier, B., Proust, J.N., Baltzer, A., Sorrel, P., Traini, C., 2010. The Holocene

605   transgression as recorded by incised-valley infilling in a rocky coast context with low

606   sediment supply (southern Brittany, western France). Bulletin de la Société

607   Géologique de France 181 (2), 115–128.

608   Menier, D., Augris, C., Briend, C., 2014. Les réseaux fluviatiles anciens du plateau

609   continental de Bretagne Sud. Ed. QUAE, 104 p.

610   Metcalfe, I., 2011. Tectonic framework and Phanerozoic evolution of Sundaland. Gondwana

611   Research, 19(1), pp.3-21.

612   Mitchum, R.M. and Vail, P.R., 1977. Seismic stratigraphy and global changes of sea-level,

613   part 7. Seismic stratigraphic interpretation procedure. AAPG Memoir 26, 135-143.

614   Moreira, D.A., Gomes, M.P. & Vital, H., 2019. Shallow sedimentation of Natal shelf and

615   coastal erosion implications, NE Brazil. Geo-Marine Letters 40, 843-851.

616   Nordfjord, S., Goff, J.A., Austin, J.A., Gulick, S.P.S., 2006. Seismic facies of incised-valley

617   fills, New Jersey continental shelf: implications for erosion and preservation processes

acting during latest Pleistocene–Holocene transgression. Journal of Sedimentary Research 76, 1284-1303.

Patmosukismo, S. and Yahya, I., 1974. The basement configuration of the Northwest Java area. Proceeding of the Third Annual Convention, Indonesian Petroleum Association, 129-152.

Posamentier, H.W., 2001. Lowstand Alluvial Bypass Systems: Incised vs. Unincised. AAPG Bulletin 85 (10), 1771–1793.

Posamentier, H.W. and Allen, G.P., 1999. Siliciclastic sequence stratigraphy: concepts and applications. SEPM Concepts in Sedimentology and Paleontology 9, 210 p.

Puchala, R.J., Porębski, S.J., Śliwiński, W.R., August, C.J., 2011. Pleistocene to Holocene transition in the central basin of the Gulf of Thailand, based on geoacoustic survey and radiocarbon ages. Marine Geology 288, 103-111.

Reineck, H.E., Singh, I.B., 1980. Depositional Sedimentary Environments, second ed. Springer-Verlag, New York, 430 pp.

Sarr, A.-C., Husson, L., Sepulchre, P., Pastier, A-M., Pedoja, K., Elliot, M., Arias-Ruiz, C., Solihuddin, T., Aribowo, S., Susilohadi, 2019. Subsiding Sundaland. Geology 47 (2), 119-122.

Sathiamurthy, E., Voris, H.K., 2006. Maps of Holocene Sea Level Transgression and Submerged Lakes on the Sunda Shelf. The Natural History of Chulalongkorn University, Supplement 2:1-43.

Sathiamurthy, E., Rahman, M.M., 2017. Late Quaternary paleo fluvial system research of Sunda Shelf: A review. Bulletin of the Geological Society of Malaysia 64, 81-92.

640   Shennan, I., 2018. Sea Level Studies – Overview. Reference Module in Earth Systems and

641   Environmental Sciences, Elsevier. https://doi.org/10.1016/B978-0-12-409548-

642   9.11063-2.

643   Schubel, J.R., 1974. Gas bubbles and the acoustically impenetrable, or turbid, character of

644   some estuarine sediments. In: Kaplan, I.R. (Ed.), Marine Science, Vol. 3. Plenum Press, New

645   York, pp. 275–298.

646   Smith, D.E., Harrison, S., Firth, C.R., Jordan, J.T., 2011. The early Holocene sea level rise.

647   Quaternary Science Reviews 30, 1846-1860.

648   Suter, J.R., Berryhill, H.L., Penland, S., 1987. Late Quaternary sea level fluctuations and

649   depositional sequences, Southwest Louisiana continental shelf. In: Nummedal, D.,

650   Pilkey, O.H., Howard, S.D. (Eds.), Sea Level Fluctuation and Coastal Evolution.

651   SEPM Special Publication 41, pp. 199 – 219.

652   Suyanto, F.X. and Sumantri, Y.R., 1977, Preliminary study on the Tertiary depositional

653   patterns of Java: 6th Annual Convention Proceedings Indonesian Petroleum

654   Association 2, 183–213.

655   Tesson, M., Posamentier, H.W., Gensous, B., 2000. Stratigraphic organization of Late

656   Pleistocene deposits of the western part of the Golfe du Lion Shelf (Langedoc Shelf),

657   western Mediterranean Sea, using high-resolution seismic and core data. American

658   Association of Petroleum Geologists Bulletin 84, 119–150.

659   Tesson, M., Labaune, C., Gensous, B., Delhaye-Prat, V., 2010. Quaternary compound incised

660   valleys of the Roussillon coast (SE France): correlation of seismic data with core data

661   Bulletin de la Société Géologique de France 181 (2), 183–196.

662 Tesson, M., Posamentier, H.W., Gensous, B., 2015. Compound incised-valley

663   characterization by high-resolution seismics in a wave-dominated setting: Example of

664   the Aude and Orb rivers, Languedoc inner shelf, Gulf of Lion, France. Marine

665   Geology 367, 1-21.

666 Thomas, M.A. and Anderson, J.B., 1994. Sea-level controls on the facies architecture of the

667   Trinity/Sabine incised-valley system, Texas continental shelf, in Dalrymple, R.W.,

668   Boyd, R., and Zaitlin, B.A., Incised-Valley Systems: Origin and Sedimentary

669   Sequences: SEPM, Special Publication 51, 63–82.

670 Twarog, M.R., Culver, S.J., Mallinson, D.J., Leorri, E., Donovan, B., Harrison, E.I., Hindes,

671   H., Reed, D., Horsman, E., Shazili, N.A.M., Parham, P.R., 2021. Depositional

672   environments and sequence stratigraphy of post-last glacial maximum incised valley-

673   fill, Malay Basin, northern Sunda Self. Marine Geology 436, 106457.

674 Voris, H.K., 2000. Maps of Pleistocene sea levels in Southeast Asia: shorelines, river systems

675   and time durations. Journal of Biogeography 27, 1153-1167.

676 Wang, R., Colombera, L., Nigel, P., Mountey, P., 2020. Quantitative analysis of stratigraphic

677   architecture of incised-valley fills: A global comparison of Quaternary systems. Earth

678   Science Reviews 200, 102988.

679 Zahirovic, S., Flament, N., Muller, R.., Seton, M., Gurnis, M., 2016. Large fluctuations of

680   shallow seas in low-lying Southeast Asia driven by mantle flow. Geochemistry,

681   Geophysics, Geosystems 17 (9), 3589-3607.

682

683 **Caption Figures**

684   **Figure 1. A:** Map showing the spatial distribution and type of vegetation cover in Sundaland

685   during the LGM. Figure adapted from Heaney (1991), Voris (2000) and Bird et al. (2005). **B:**

686   Location of seismic lines in the Java Sea and also shown are the bathymetry contours. **C:**

687   Location of seismic lines and boreholes used in this study from the Jakarta Bay.

688   **Figure 2. A.** Map of the Java Sea seafloor sediments. **B.** Map of seafloor sediments of the

689   Jakarta Bay (Harkin, et al., 2004) and geology of the Jakarta-Tangerang area.

690   **Figure 3.** Map showing the bathymetry and morphobathymetric features of the Java Sea and

691   the Indian Ocean. Also shown is the drainage basins and the fluvial network of Java. Note the

692   large drainage basins in the north and the smaller basins in the south. The southeastern limit

693   of the Sunda Shelf is visible at the ~110 m

694   **Figure 4. A:** Sparker 2D High Resolution Seismic profile L-42. The profile passes through

695   cores BH-02 and BH-07, south to north in the Jakarta Bay. Vertical scale in two-way travel

696   time in seconds (TWTs). The scale in meters is established for sediments with P-wave

697   velocity of 1600 m/sec. **B:** Sparker 2D High Resolution Seismic profile CL-06, west to east in

698   the Jakarta Bay. Vertical scale in two-way travel time in seconds (TWTs). The scale in meters

699   is established for sediments with P-wave velocity of 1600 m/sec.

700   **Figure 5.** Sparker 2D High Resolution Seismic profiles C-8, C-7 and C-X. The profile C-8 is

701   located in. Vertical scale is in two-way travel time in seconds (s TWT). The scale is in meters

702   and is established for sediments with P-wave velocity of 1600 m/sec.

703   **Figure 6.** Stratigraphic correlation of the facies types recognized in the sediment cores and

704   interpretation of corresponding depositional environments. Also shown are the stratigraphic

705   positions of samples used for AMS ^{14}C dating.

706   **Figure 7.** Microfossil assemblages that aided in the interpretation of the depositional

707   environments of the sediments. Benthic foraminifera: 1. *Asterorotalia*; 2. *Operculina*; 3 & 7

708 *Pseudorotalia*; 4. *Quinqueloculina*; 5 & 6. *Elphidium*; 8-10. *Ammonia yabei.* Ostracoda: 11.

709 *Phlyctenophora*; 12. *Neocytheretta*; 13. *Loxoconcha*; 14. *Keijella*; 15. *Neomonoceratina*; 16

710 *Hemicytheridea*

711 **Figure 8. A:** Reconstructed paleochannel network of the offshore Java Sea based on High

712 Resolution seismic profiles (location of all lines shown in 1B). **B:** Time slice from the north

713 of the study area at ~72 m subsea showing the principal trunk incised valley and associated

714 components of the fluvial system such as incised dendritic tributary valleys, scroll bars and

715 abandoned meander loops. Figure modified from Posamentier (2001).

716 **Figure 9.** Regime diagram showing the global eustatic sea level and Sunda shelf sea level

717 curve for the past 125 ka and 20 ka, respectively, along with timing of the major Marine

718 Isotopic Stages (1–5) and the Last Glacial Maximum. Sunda shelf sea-level curve is adapted

719 from Twarog et al. (2021). Red stars indicate the calibrated ages of sedimentary units (shown

720 with white circles and U7–4) from ^{14}C radiocarbon dating of shells, shell fragments and

721 sediments.

722 **Figure 10. A:** Present-day sedimentary architecture of the northern Java Sea. **B:** Schematic

723 depiction of the evolution of incised valley fill in Java Sea, modified from Posamentier

724 (2001). It shows from the time of maximum sea level lowstand, (A) sedimentation was

725 characterized by fluvial deposition, (B) followed by rapid transgression and filling by traction

726 and hemipelagic sedimentation, and finally, (C) the time of sea-level highstand and deposition

727 of hemipelagic drape over the entire area.

728

729 **List of Tables**

730 **Table 1.** Locations, water depth and lengths of sediment cores recovered from the the Jakarta

731 Bay and analysed in this study

732 **Table 2.** AMS ^{14}C dating of shells, shell fragments and sediments retrieved from the cores

733 **Table 3.** Characteristics of acoustic facies and seismic units and their interpretation in terms

734 of depositional environments.

735 **Table 4.** Microfossil abundances in BH-02 and BH-07

736

737

738

739

740

741

742

743 **Figures**
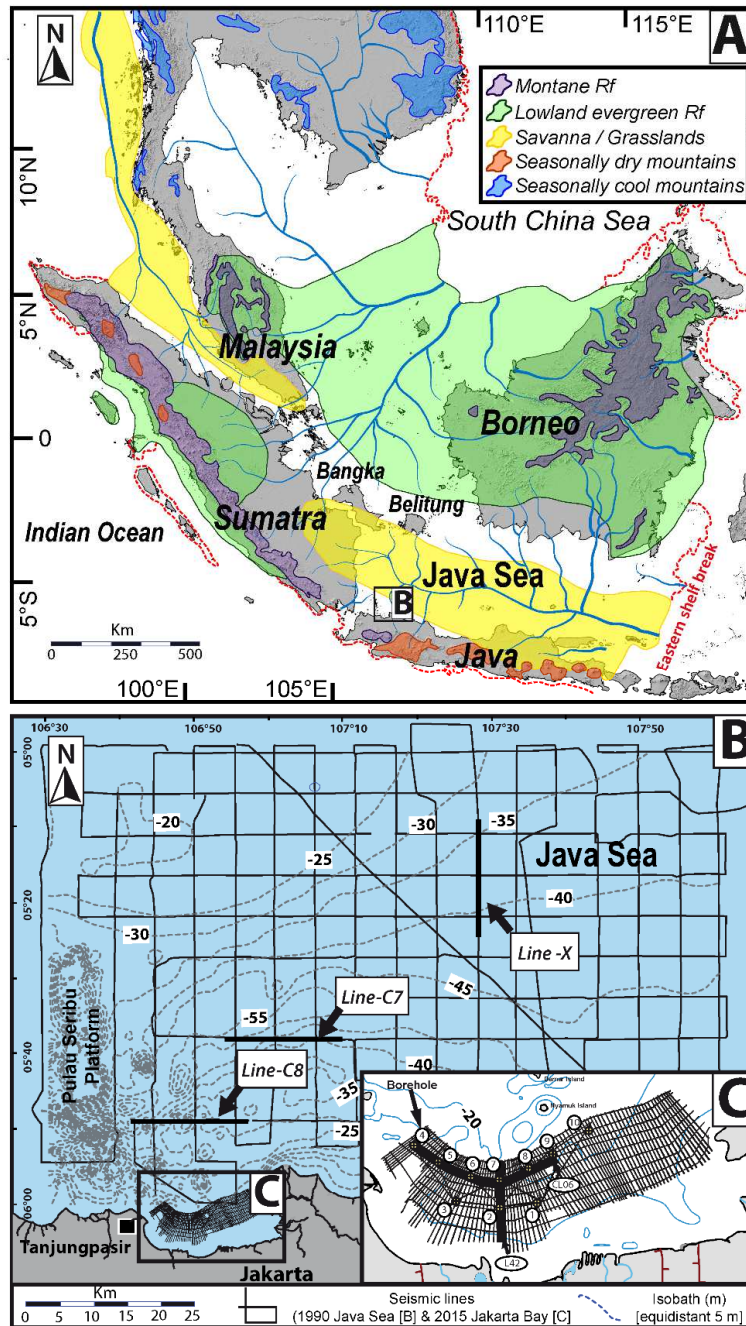
744

Figure 1. A: Map showing the spatial distribution and type of vegetation cover in Sundaland

during the LGM and red dashed line shows the approximate spatial extent of exposed

landmass of Sundaland during the LGM. Figure adapted from Heaney (1991), Voris (2000)

and Bird et al. (2005). **B:** Location of seismic lines in the Java Sea and also shown are the

bathymetry contours. **C:** Location of seismic lines and boreholes used in this study from the

Jakarta Bay.

Figure 2. A. Map of the Java Sea seafloor sediments. **B.** Map of seafloor sediments of the

Jakarta Bay (Harkin, et al., 2004) and geology of the Jakarta-Tangerang area.

755

756
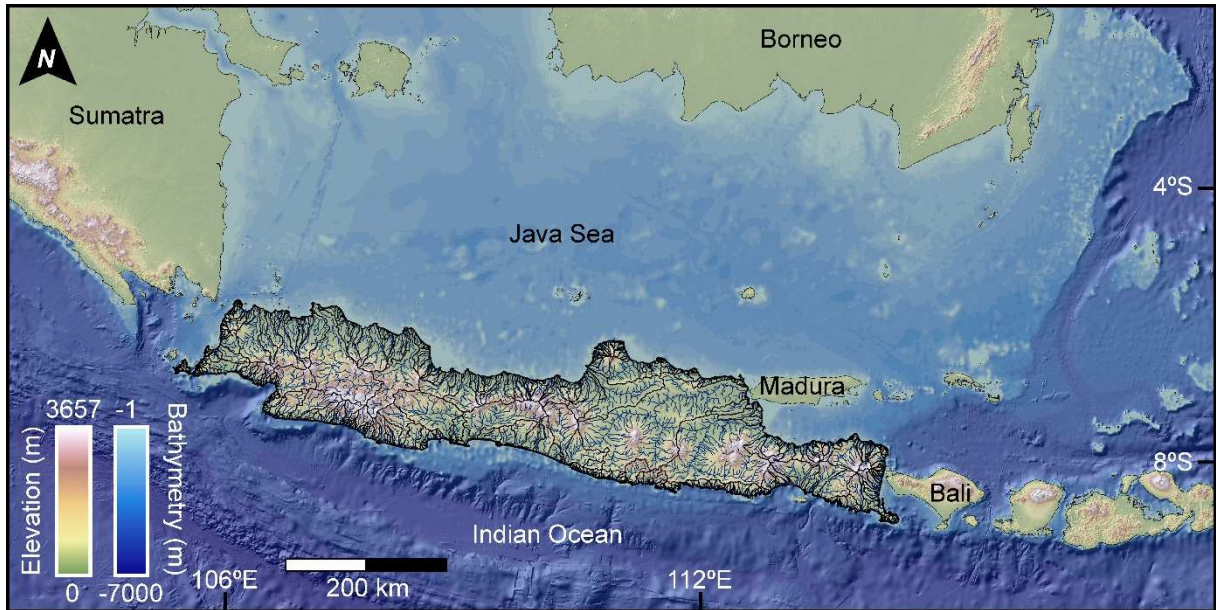
Figure 3. Map showing the bathymetry and morphobathymetric features of the Java Sea and the Indian Ocean. Also shown is the drainage basins and the fluvial network of Java. Note the large drainage basins in the north and the smaller basins in the south. The southeastern limit of the Sunda Shelf is visible at the ~110 m

761
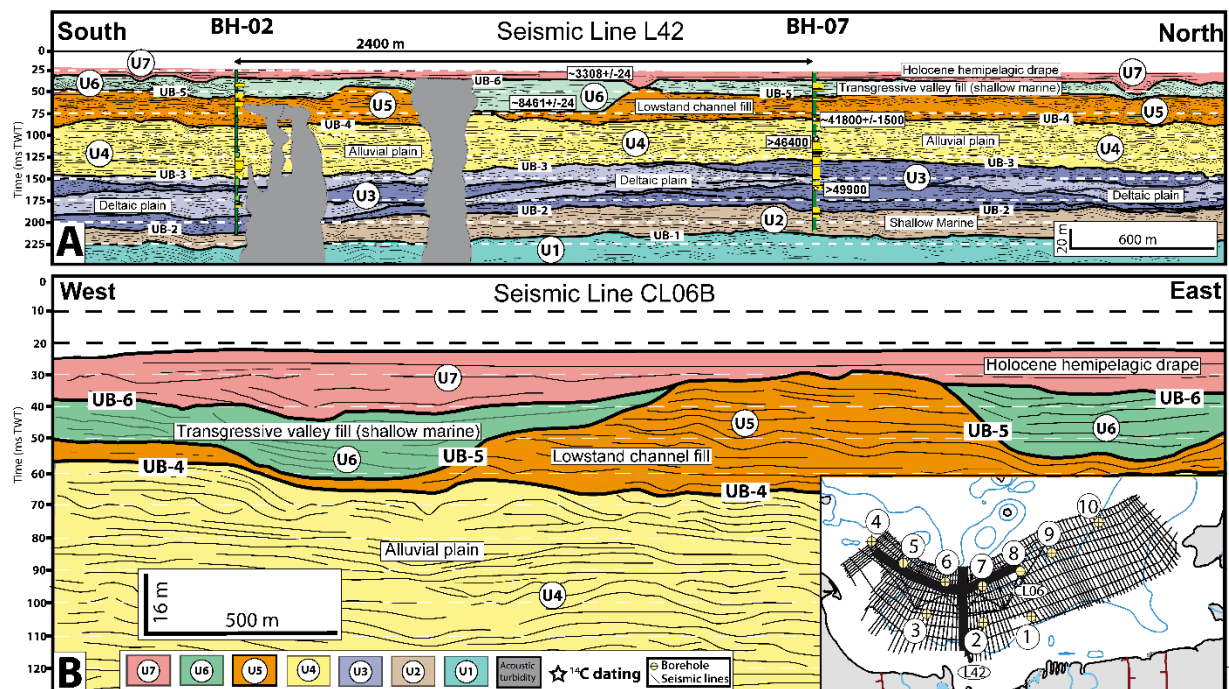
Figure 4. A: Sparker 2D High Resolution Seismic profile L-42. The profile passes through cores BH-02 and BH-07, south to north in the Jakarta Bay. Vertical scale in two-way travel

time in seconds (TWTs). The scale in meters is established for sediments with P-wave velocity of 1600 m/sec. Note that the light blue coloured packages within U3 indicate the head of several deltaic lobes that are stacked and extends laterally. **B:** Sparker 2D High Resolution Seismic profile CL-06, west to east in the Jakarta Bay. Vertical scale in two-way travel time in seconds (TWTs). The scale in meters is established for sediments with P-wave velocity of 1600 m/sec.
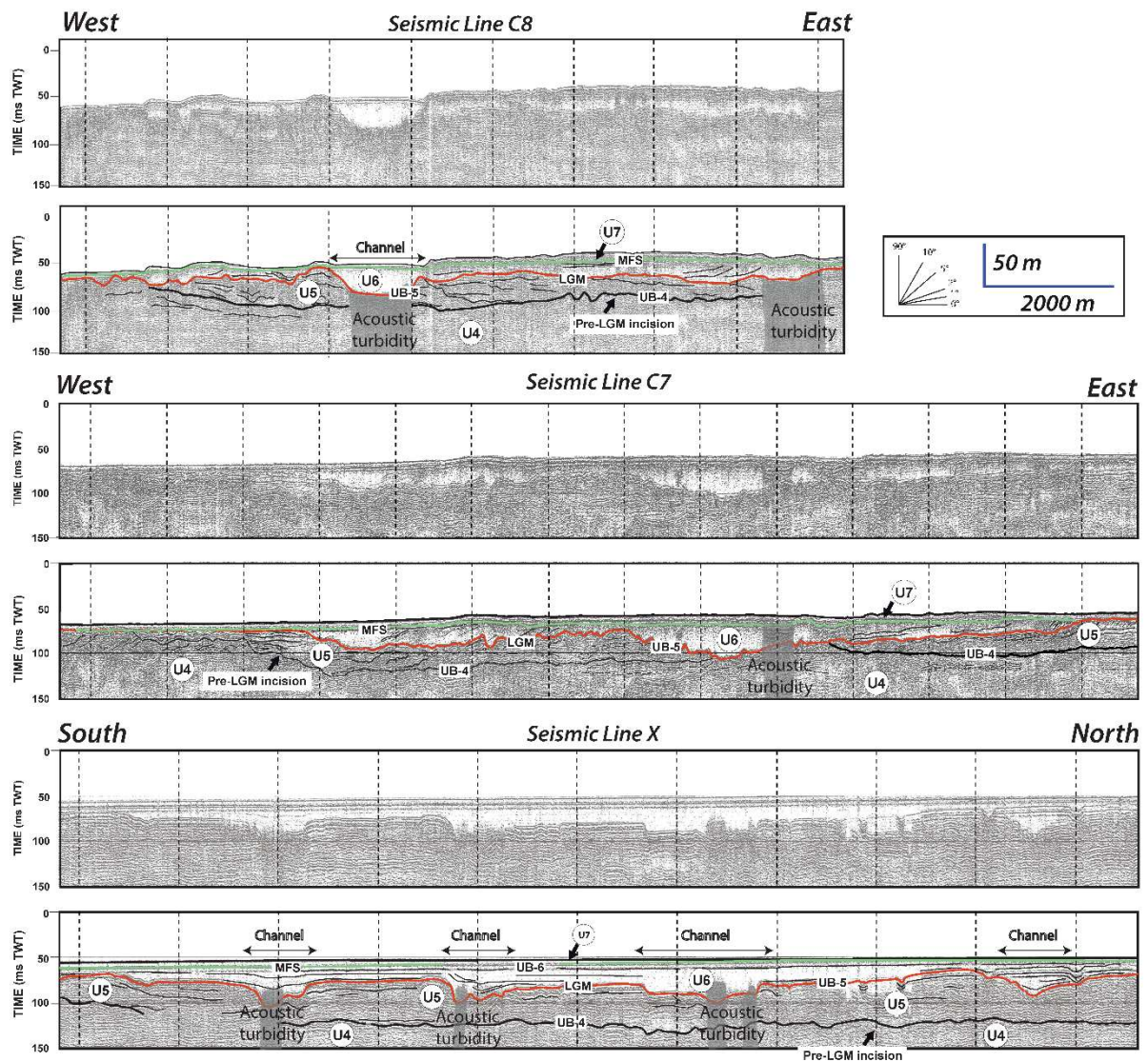
Figure 5. Sparker 2D High Resolution Seismic profiles C-8, C-7 and C-X. The profile C-8 is located in. Vertical scale is in two-way travel time in seconds (s TWT). The scale is in meters and is established for sediments with P-wave velocity of 1600 m/sec.

775
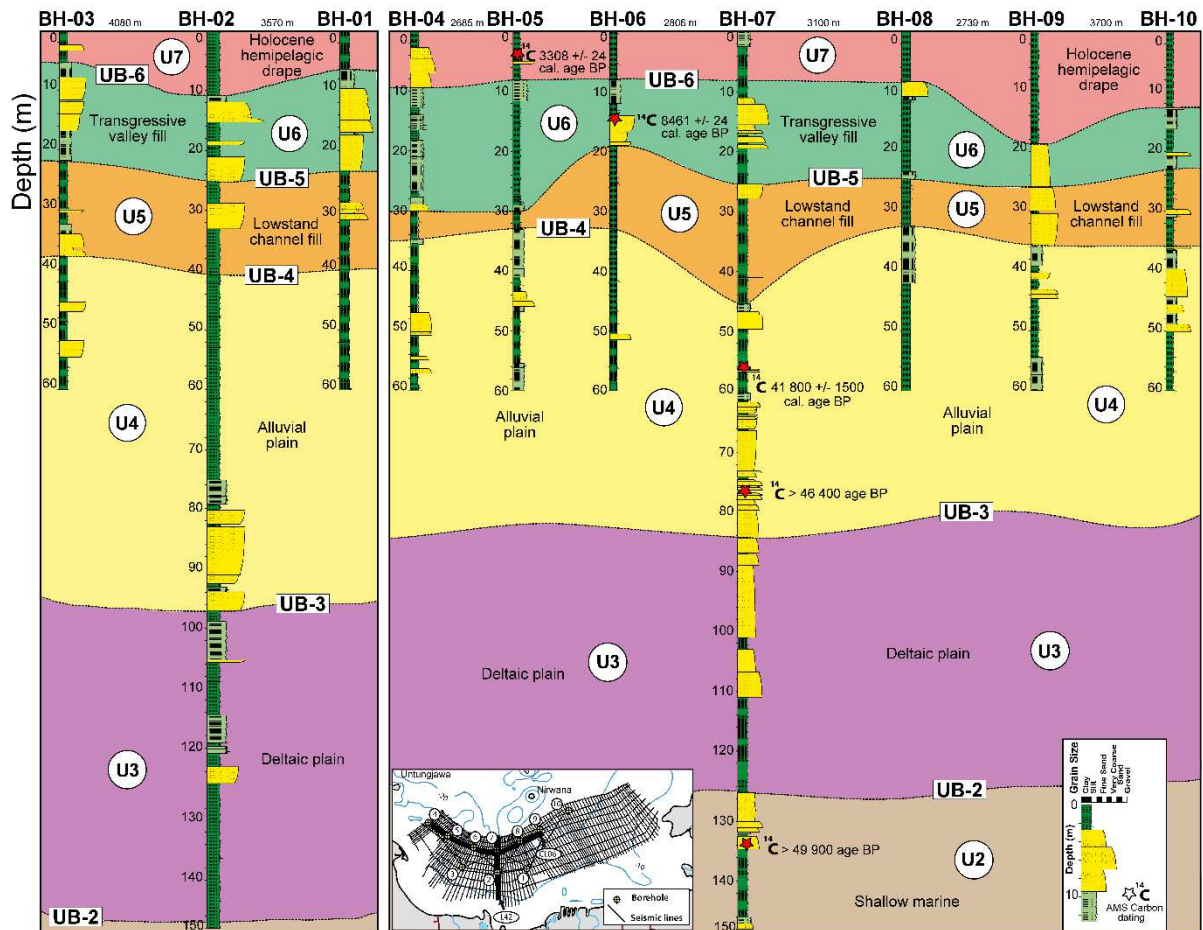
776

777

778

779

Figure 6. Stratigraphic correlation of the facies types recognized in the sediment cores and interpretation of corresponding depositional environments. Also shown are the stratigraphic positions of samples used for AMS ^{14}C dating.

783

784

785

786

787

788

789
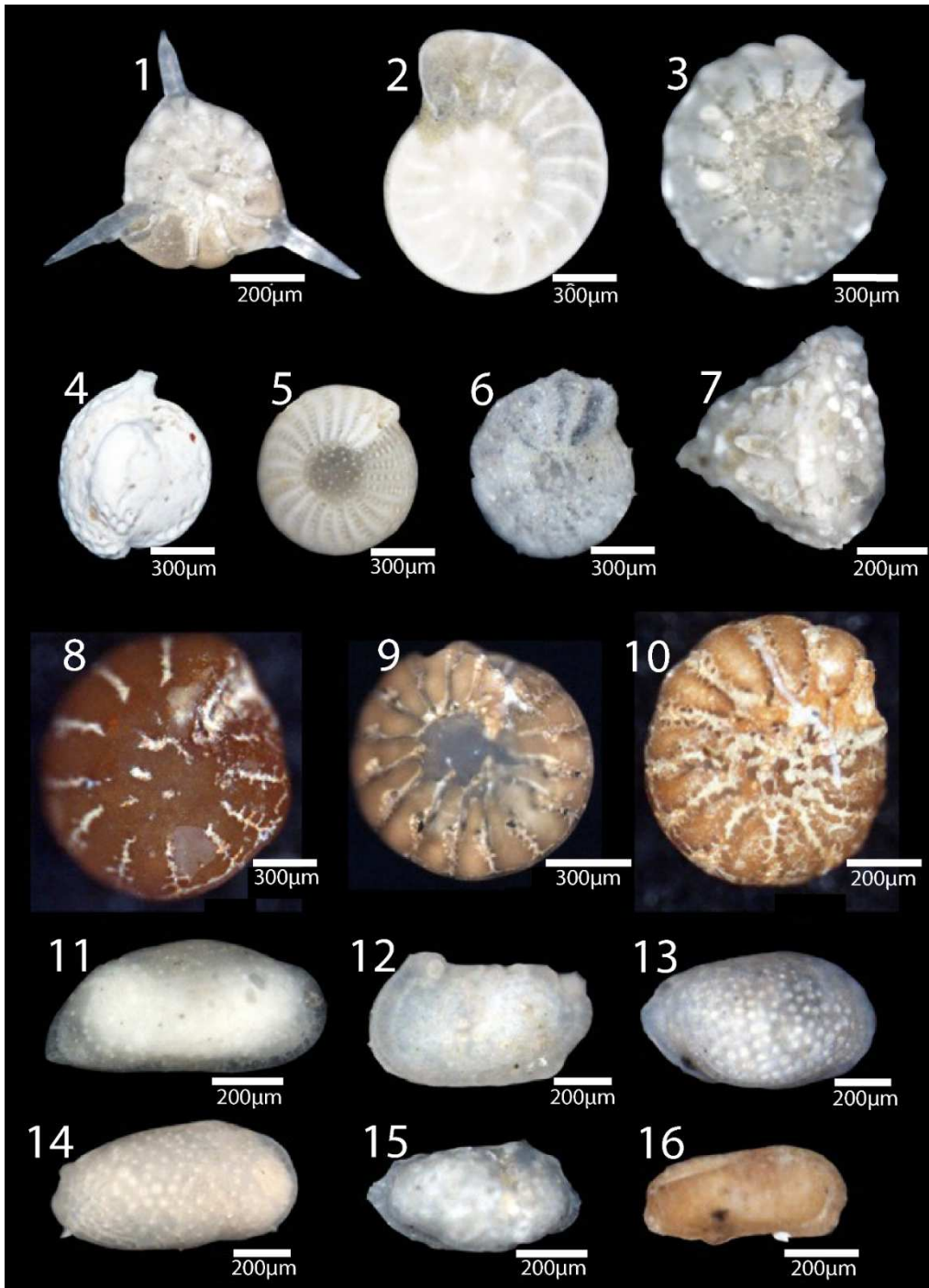
790

791 **Figure 7.** Microfossil assemblages that aided in the interpretation of the depositional

792 environments of the sediments. Benthic foraminifera: 1. *Asterorotalia*; 2. *Operculina*; 3 & 7

793 *Pseudorotalia*; 4. *Quinqueloculina*; 5 & 6. *Elphidium*; 8-10. *Ammonia yabei.* Ostracoda: 11.

794 *Phlyctenophora*; 12. *Neocytheretta*; 13. *Loxoconcha*; 14. *Keijella*; 15. *Neomonoceratina*; 16

795 *Hemicytheridea*
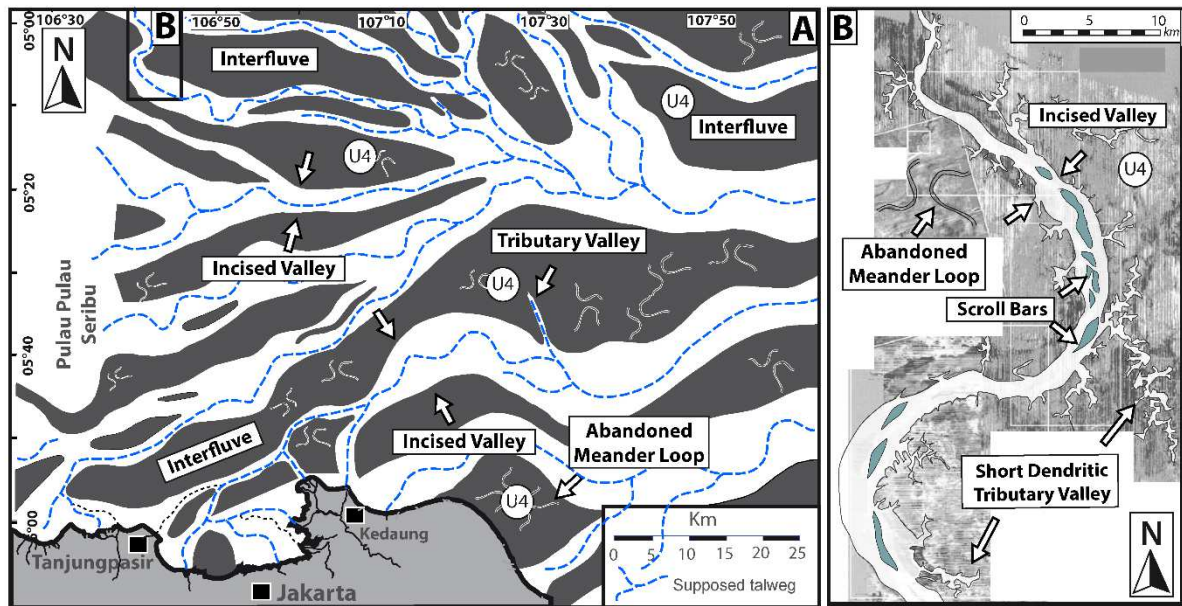
796

797 **Figure 8. A:** Reconstructed paleochannel network of the offshore Java Sea based on High

798 Resolution seismic profiles shown in Figure 1B. **B:** Time slice from the north of the study

799 area at ~72 m subsea showing the principal trunk incised valley and associated components of

800 the fluvial system such as incised dendritic tributary valleys, scroll bars and abandoned

801 meander loops. Figure modified and location from Posamentier (2001)

802

803

804

805

Figure 9. Regime diagram showing the global eustatic sea level and Sunda shelf sea level curve for the past 125 ka and 20 ka, respectively, along with timing of the major Marine Isotopic Stages (1–5) and the Last Glacial Maximum. Sunda shelf sea-level curve is adapted from Twarog et al. (2021). Red stars indicate the calibrated ages of sedimentary units (shown with white circles and U7–4) from ^{14}C radiocarbon dating of shells, shell fragments and sediments.

Figure 10. A: Present-day sedimentary architecture of the northern Java Sea. **B:** Schematic

depiction of the evolution of incised valley fill in Java Sea, modified from Posamentier

(2001). It shows from the time of maximum sea level lowstand, (A) sedimentation was

characterized by fluvial deposition, (B) followed by rapid transgression and filling by traction

and hemipelagic sedimentation, and finally, (C) the time of sea-level highstand and deposition

of hemipelagic drape over the entire area.

829 **Tables**

830 **Table 1. Locations, water depth and lengths of sediment cores recovered from the the**

831 **Jakarta Bay and analysed in this study**

Core	Core length (m)	Water depth (m)	Coordinates			
			WGS_1984_UTM_Zone_48S		Latitude (S)	Longitude (N)
			X (m)	Y (m)		
1	60	15.31	704259.24	9330033.60	6°3'28.92"	106°50'43.98"
2	150	14.72	700755.12	9329627.65	6°3'42.52"	106°48'50.09"
3	60	13.76	696699.08	9330108.06	6°3'27.30"	106°46'38.15"
4	60	14.46	692826.95	9335232.98	6°0'40.92"	106°44'31.67"
5	60	15.27	695034.37	9333810.38	6°1'26.97"	106°45'43.62"
6	60	16.54	697886.62	9332414.95	6°2'12.11"	106°47'16.50"
7	150	17.36	700646.47	9332020.42	6°2'24.64"	106°48'46.28"
8	60	18.23	703556.3	9334974.58	6°1'49.40"	106°50'20.78"
9	60	19.59	705541.07	9334974.41	6°0'47.30"	106°51'25.11"
10	60	20.49	708651.68	9336919.69	5°59'44.30"	106°53'6.01"

832

833 **Table 2. AMS ^{14}C dating of shells, shell fragments and sediments retrieved from the**

834 **cores**
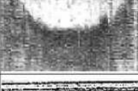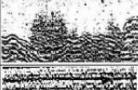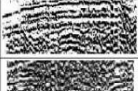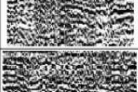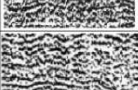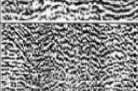
Core	Lab number	Depth (mbss)	Seismic Unit	d13C value	Age (^{14}C years BP)	Material
BH-05	X32132	7	U7	3.5	3308±24	Shell
BH-06	X32133	14.3	U6	-4.0	8461±29	Shell
BH-07	X31404	56.2	U4	-29.1	41800±1500	Sediment and shell fragments
	X31405	77.00	U4	-19.2	>46400	Sediment and shell fragments
	X31406	134.45	U2	0.8	>49900	Sediment and shell fragments

835

836

837

838

Table 3. Characteristics of acoustic facies and seismic units and their interpretation in terms of depositional environments.

Unit	Facies	Illustration	Continuity	Amplitude	Frequency	Reflector Configuration	Interpretation
U-7	F-7A		Good	Good	Medium	Aggrading parallel	Marine muds
	F-7B		Medium	Good	Medium	Aggrading parallel	Channel fill
U-6	F-6A		Poor	Very poor	Low	Transparent	Channel infill polymix
	F-6B		Poor	High	Low	Acoustic turbidity	Gas-charged sediments
	F-6C		Poor	Medium	High	Aggrading parallel	Bars associated to channel migration
U-5	F-5A		Very poor	Medium	Low	Acoustic turbidity	Gas-charged sediments
	F-5B		Poor	Medium	High	Oblique-aggrading subparallel	Channel bars system
	F-5C		Poor	High	High	Oblique-aggrading subparallel	Channel bars system
U-4	F-4A		Medium	Medium	High	Aggrading subparallel	Bars associated to channeling drainage system
	F-4B		Poor	Medium	Medium	Acoustic turbidity	Gas-charged sediments
	F-4C		Poor	Poor	Medium	Irregular Oblique-aggrading subparallel	Bars associated to channeling drainage system
U-3	F-3A		Medium	Medium	Medium	Aggrading sub parallel	Marine muds and sandy intercalation
	F-3B		Very poor	Medium	Medium	Acoustic turbidity	Gas-charged sediments
U-2	F-2A		Medium	Medium	Low	Aggrading folded parallel	Marine muds
	F-2B		Very poor	Medium	Low	Acoustic turbidity	Gas-charged sediments
U-1	F-1A		Low	Medium	Low	Aggrading sub-parallel	Marine sediments
	F-1B		Very poor	Low	Low	Acoustic turbidity	Gas-charged sediments

Table 4. Microfossil abundances in BH-02 and BH-07

BH-02

BH-02 depth below seafloor (m)	Ostracod																			Benthic foraminifera																		Remarks
	Actinocythereis	*Argilloecia*	*Aljehella semiplicata*	*Bairdopillata*	*Caudites*	*Cytherella*	*Cytherelloidea*	*Hemicytheridea*	*Keijella*	*Keijia*	*Lanckacythere*	*Mxcyprideis*	*Neomonocertina*	*Loxoconcha*	*Phlyctenophora*	*Pistocythereis*	*Psammocythere*	*Stigmatocythere*	*Other*	*Ammonia*	*Amphistegina*	*Asterorotalia*	*Brizalina*	*Cancris*	*Dendritina*	*Discopulvinulina*	*Elphidium*	*Florilus*	*Lagena*	*Operculina*	*Pseudorotalia*	*Quinqueloculina*	*Rotalia*	*Shlumbergerella*	*Spiroloculina*	*Triloculina*	*Other*	
3,20			○			○	○	A	●		°		●	©	A	°			©	●					°		A	°			©	A	°		°			Shallow marine environment
7,18	°	°	°		○	○		●	●				©	A	●	○			°	●		○			©		●			●		●			©	°	°	
11,03						○	°							°											©							○						
20,90	○					°		○	A		A		A	°		A				○		●			A		○			©	©				°			
27,25																																						land
41,00																																						
42,00																																						
54,65																									°					●		°						Shallow marine environment
71,00									°																					°								
110,70	○					©	©						○							●		○									○							
120,00	○																					○								○						°		
128,50	°	©	○	○		A	©	A	©	©			©	○			°	°		A		●	○		○		○			○		©	A			°		
134,64		○	○	°	°		○	○	°	○			°	○						A	°	A					©					○	©			°		

Notes:
Biogenic
- Rare (R) : 1 — ○
- Few (F) : 2-5 — ○
- Common (C) : 6-10 — ©
- Abundant (A) : 11-25 — A
- Very abundant (VA) : >25 — ●

3.20 m   27.25 m   54.65m   110.70m   134.64 m

BH-07

BH-07 Depth below seafloor (m)	Ostracod																		Benthic foraminifera																Remarks
	Actinocythereis	*Argilloecia*	*Aljehella*	*Cytherella*	*Cytherelloidea*	*Cytheropteron*	*Hemicytheridea*	*Keijella*	*Keijia*	*Neomonocertina*	*Neocytherettha*	*Loxoconcha*	*Phlyctenophora*	*Pistocythereis*	*Stigmatocythere*	*Mxcyprideis*	*Other*	*Ammonia*	*Asterorotalia*	*Brizalina*	*Cancris*	*Cibicides*	*Dendritina*	*Elphidium*	*Florilus*	*Lenticulina*	*Operculina*	*Pseudorotalia*	*Quinqueloculina*	*Spiroloculina*	*Triloculina*	*Other*	
2,10	©	°	○	©	°	A	°	©		°	○		A	°	°			○				A		●		A	°	A	○	A	°		shallow marine-reef environments
3,18	○		°		○	°			°		°	°					○				A		●		A	A	A					
22,68	°	°	°	°	©	●		°	A	○	○	A	A	○	○	°		●					●			○	○	°	○		°	
23,40	○	°	○	°	©			°	●	○	©	A	A	○	○	°		○					●			○		©			°	
23,85	©	©	©		○	A		●	°	©	°	°	69	©	©	°		○	°					●			○		A	○	°	
26,10										○								°					○	○		©		°				nearshore
27,45										○								○					○									
27,50																																
28,30																										°						
31,80	○		○						○			○	○	°				○		°			○	A		○	○	A	○			
32,62																							°	○								
33,45																																
38,30																								°								nearshore
40,75																							○	°		©	©	°				
53,27																		A	A				©	©	°							
55,65	○			○	°					○	°							°					●	©	©	©		A				
56,20																																Barren zone, no ostracod n foram, quartz sand, organic materials
65,11																																
68,55																																
71,72																																
77,00																																
98,40	○		○		○	○					○		○				°	●	©	○	°		A				©		°			Shallow marine-reef environments
101,10	○		©	○		○	A			°	©							A	●				©	°	○		○	©	○	○		
132,84			○				°			○								A	○				34			°	©	©			A	
134,45																		●	●				>>								
136,55		A	○		○	©	○		○									●	●	°	○		○				°				
141,10			○															○	○		○		°		○		©	○			
149,41		°	○	©		©	°		°									©	●				○				©	°			

Biogenik
- Rare (R) : 1 — ○
- Few (F) : 2-5 — ○
- Common (C) : 6-10 — ©
- Abundant (A) : 11-25 — A
- Very abundant (VA) : >25 — ●

2.10 m   23.40 m   33.40 m   77.00 m   98.40 m   149.41 m